Time-retarded damping and magnetic inertia in the Landau-Lifshitz-Gilbert equation self-consistently coupled to electronic time-dependent nonequilibrium Green functions

Utkarsh Bajpai and Branislav K. Nikolić*
Department of Physics and Astronomy, University of Delaware, Newark, Delaware 19716, USA

(Received 6 December 2018; revised manuscript received 8 March 2019; published 4 April 2019)

The conventional Landau-Lifshitz-Gilbert (LLG) equation is a widely used tool to describe the dynamics of local magnetic moments, viewed as classical vectors of fixed length, with their change assumed to take place simultaneously with the cause. Here we demonstrate that recently developed [M. D. Petrović *et al.*, Phys. Rev. Appl. **10**, 054038 (2018)] self-consistent coupling of the LLG equation to a time-dependent quantum-mechanical description of electrons—where nonequilibrium spin density from time-dependent nonequilibrium Green function (TDNEGF) calculations is inserted within a torque term into the LLG equation while local magnetic moments evolved by the LLG equation introduce time-dependent potential in the quantum Hamiltonian of electrons—microscopically generates time-retarded damping in the LLG equation described by a memory kernel that is also spatially dependent. For sufficiently slow dynamics of local magnetic moments on the memory time scale, the kernel can be expanded into power series to extract the Gilbert damping (proportional to the first time derivative of magnetization) and magnetic inertia (proportional to the second time derivative of magnetization) terms whose parameters, however, are *time-dependent* in contrast to time-independent parameters used in the conventional LLG equation. We use examples of single or multiple local magnetic moments precessing in an external magnetic field, as well as field-driven motion of a magnetic domain wall (DW), to quantify the difference in their time evolution computed from the conventional LLG equation versus the TDNEGF+LLG quantum-classical hybrid approach. The faster DW motion predicted by the TDNEGF+LLG approach reveals that important quantum effects, stemming essentially from a finite amount of time that it takes for a conduction electron spin to react to the motion of classical local magnetic moments, are missing from conventional classical micromagnetics simulations. We also demonstrate a large discrepancy between the TDNEGF+LLG-computed numerically exact and, therefore, nonperturbative result for charge current pumped by a moving DW and the same quantity computed by a perturbative spin motive force formula combined with the conventional LLG equation.

DOI: 10.1103/PhysRevB.99.134409

I. INTRODUCTION

The conventional Landau-Lifshitz-Gilbert (LLG) equation [1–3] is the cornerstone of numerical micromagnetics [4] and atomistic spin dynamics [5] where one simulates the classical time evolution of many magnetic units coupled by exchange or magnetostatic interactions. The LLG equation

$$\frac{\partial \mathbf{m}(\mathbf{r},t)}{\partial t} = -g\mathbf{m}(\mathbf{r},t)\times\mathbf{B}_{\rm eff}(\mathbf{r},t) + \lambda_{\rm G}\mathbf{m}(\mathbf{r},t)\times\frac{\partial \mathbf{m}(\mathbf{r},t)}{\partial t} \tag{1}$$

describes the time evolution of $\mathbf{m}(\mathbf{r},t)$ as the unit vector $|\mathbf{m}| = 1$ of constant length representing the direction of the local magnetization. Here g is the gyromagnetic ratio and $\mathbf{B}_{\rm eff}$ is the sum of an external magnetic field and effective magnetic fields due to magnetic anisotropy and exchange coupling (an additional stochastic magnetic field can contribute to $\mathbf{B}_{\rm eff}$ to take into account finite-temperature effects [6]). The second term on the right-hand side of Eq. (1) is introduced phenomenologically to break the time-inversion symmetry, thereby generating a damping mechanism. The conventional intrinsic Gilbert damping $\lambda_{\rm G}$ is assumed to be materials-specific and, therefore, a time-independent parameter. It is typically computed using the so-called breathing Fermi surface [7] or torque-torque correlation formulas [8] within a single-particle quantum-mechanical framework (additional many-body processes have to be taken into account to make $\lambda_{\rm G}$ finite in the clean limit at low temperatures [9]). In the original form, Eq. (1) is written for a bulk material as a highly nonlinear partial differential equation. It can also be rewritten for a macrospin or a lattice of atomic spins leading to a system of nonlinear ordinary differential equations [5].

In the case of conducting ferromagnets, the LLG equation has to be extended by including additional terms, such as (i) spin-transfer torque [10] $\mathbf{T}\propto\langle\hat{\mathbf{s}}\rangle\times\mathbf{m}$ due to injected electrons generating nonequilibrium spin density $\langle\hat{\mathbf{s}}\rangle$ that is noncollinear to local magnetization; (ii) additional Gilbert damping, $(g_{\uparrow\downarrow}/4\pi)\mathbf{m}\times\partial\mathbf{m}/\partial t$, due to pumping of spin currents by the dynamics of $\mathbf{m}(t)$, where $g_{\uparrow\downarrow}$ is the so-called spin-mixing conductance [11]; (iii) additional *nonlocal* Gilbert damping [12–18], $\mathbf{m}\times(\mathcal{D}\cdot\partial\mathbf{m}/\partial t)$, due to spin pumping by noncollinear magnetic textures where $\mathcal{D}_{\alpha\beta} = \eta\sum_i(\mathbf{m}\times\partial_i\mathbf{m})_\alpha(\mathbf{m}\times\partial_i\mathbf{m})_\beta$ is the 3×3 damping tensor, $\partial_i = \partial/\partial_i$, and $\alpha,\beta,i\in\{x,y,z\}$; and (iv) magnetic inertia [19–25], $I\mathbf{m}\times$

*bnikolic@udel.edu

$\partial^2\mathbf{m}/\partial t^2$, of relevance to ultrafast magnetization dynamics. Like the original Gilbert damping parameter λ_G in Eq. (1), $\mathbf{T}$, $g_{\uparrow\downarrow}$, $\mathcal{D}$, and I require microscopic quantum-mechanical calculations that are often combined [8,9,26–31] with first-principles Hamiltonians of realistic materials.

Furthermore, generalizations of the LLG equation have been considered to take into account the retardation effects [32,33],

$$\frac{\partial\mathbf{m}(\mathbf{r},t)}{\partial t} = \int_0^t dt' \int d^3\mathbf{r}'\Gamma(\mathbf{r},t;\mathbf{r}',t')\mathbf{m}(\mathbf{r}',t') \times\left[-g\mathbf{B}_{\rm eff}(\mathbf{r}',t') + \lambda_G\frac{\partial\mathbf{m}(\mathbf{r}',t')}{\partial t'}\right], \quad (2)$$

by introducing a memory kernel $\Gamma(\mathbf{r},t;\mathbf{r}',t')$. The memory kernel models space-time correlation between local magnetic moments, i.e., the fact that the cause for the change of local magnetization occurs at time $t-t'$ and at position $\mathbf{r}-\mathbf{r}'$ while the effect at position $\mathbf{r}$ is visible at the later time t. It has been specified phenomenologically, such as the sum of an instantaneous and time-dependent part that decays exponentially on a characteristic time scale defining the strength of memory [32,33]. It is also often simplified [33] by considering time retardation only, $\Gamma(\mathbf{r},t;\mathbf{r}',t') \to \Gamma(t,t')$, so that any space-retardation effects are included only through the effective field $\mathbf{B}_{\rm eff}(\mathbf{r},t')$.

The time retardation described by $\Gamma(t,t')$ is a damping mechanism in addition to well-established mechanisms—the combined effects of spin-orbit coupling and electron-phonon interaction [7,8]—which govern λ_G in Eq. (1). However, the magnitude of $\Gamma(t,t')$ cannot be deduced from purely phenomenological considerations [32,33]. Instead, the introduction of the memory kernel $\Gamma(t,t')$ can be justified microscopically [6,22,34–37] by using *quantum-classical hybrid* approaches, where the time-dependent quantum formalism is used to compute $\langle\hat{\mathbf{s}}\rangle(t)$, which is then fed into the LLG equation, while in turn local magnetization from the LLG equation generates a time-dependent field in the quantum Hamiltonian of electrons. Although electron dynamics is assumed to be much faster than that of local magnetic moments, it still takes finite time for electron spin to react to the new position of $\mathbf{m}(\mathbf{r},t)$. This is the fundamental reason for time-retarded damping effects encoded by Eq. (2), which are present even if the intrinsic Gilbert damping in Eq. (1) is vanishingly small due to small spin-orbit coupling (nonzero λ_G requires spin-orbit coupling [7–9] and scales quadratically with it [38]). Since classical micromagnetics simulations typically use only the conventional intrinsic Gilbert damping term in Eq. (1), while not considering explicitly the flow of conduction electrons in the presence of magnetization dynamics, the question arises about the magnitude of neglected effects such as time-retarded damping in standard simulations of magnetic-field- or current-driven dynamics of noncollinear magnetic textures such as magnetic domain walls (DWs) [39–47] and skyrmions [48,49].

Although quantum-classical approaches, which automatically include time-retardation effects, have been discussed previously [6,22,34–37], they have been focused on the simple examples in which one or two local magnetic moments (pertinent to, e.g., magnetic molecules) interact with either a closed electronic quantum system [22,35] (i.e., not attached to macroscopic reservoirs to allow electron spin and charge currents to flow into and from an external circuit) or an open electronic quantum system but employing approximations [6,34,36,37] to obtain an analytical solution. Thus, these approaches are not suitable for simulations of spintronic devices containing a large number of noncollinear local magnetic moments.

Here we employ a recently developed [50] *numerically exact and, therefore, nonperturbative* algorithm combining the time-dependent nonequilibrium Green function formalism [51,52] with the conventional LLG Eq. (1) (TDNEGF+LLG) to demonstrate how it effectively generates time-retardation effects, whose memory kernel can be explicitly extracted in terms of TDNEGFs only in some limits (such as weak electron-spin/local-magnetic-moment interaction and weak coupling of the active region to macroscopic reservoirs). The paper is organized as follows. Section II A introduces a model quantum Hamiltonian for an electronic subsystem and a classical Hamiltonian for the subsystem comprised of local magnetic moments. In Sec. II B, we show how the nonequilibrium expectation value of spin density,

$$\langle\hat{\mathbf{s}}\rangle^i(t) = \frac{\hbar}{2}\mathrm{Tr}\,\{[\boldsymbol{\rho}_{\rm neq}(t) - \boldsymbol{\rho}_{\rm eq}]\,|i\rangle\,\langle i|\otimes\boldsymbol{\sigma}\}, \quad (3)$$

inserted into the LLG Eq. (1) generates a memory kernel because of the structure of the nonequilibrium time-dependent density matrix $\boldsymbol{\rho}_{\rm neq}(t)$ obtained from TDNEGF calculations. Here $\boldsymbol{\rho}_{\rm eq}$ is the grand-canonical equilibrium density matrix, $\boldsymbol{\sigma} = (\hat{\sigma}^x, \hat{\sigma}^y, \hat{\sigma}^z)$ is the vector of the Pauli matrices, $|i\rangle$ is the electron orbital centered on site i, and the operator $|i\rangle\,\langle i|\otimes\boldsymbol{\sigma}$ acts in the composite Hilbert space $\mathscr{H} = \mathscr{H}_{\rm orb}\otimes\mathscr{H}_{\rm spin}$ of the electronic orbital and spin degrees of freedom. In this section, we also discuss how in the limit of slow magnetization dynamics the memory kernel can be expanded in a Taylor series in order to extract conventional Gilbert damping and magnetic inertia terms, but with time- and spatially dependent parameters $\lambda_i^{\rm D}(t)$ and $I_i^{\rm D}(t)$. In Sec. II C we introduce the theory for calculating Gilbert damping (λ_S) using the S-matrix theory, which describes the dynamics of local magnetic moments using collective coordinates, and later we compare it with our dynamical Gilbert damping. In Secs. III A–III C we compare the dynamics of local magnetic moments driven by an external magnetic field as computed by TDNEGF+LLG versus conventional LLG simulations for three one-dimensional (1D) examples depicted in Figs. 1(a)–1(c), respectively. Section III C also compares pumped charge current due to the DW motion as computed by TDNEGF+LLG versus the widely used spin motive force (SMF) theory [12,53] combined [54–56] with the conventional LLG equation. We conclude in Sec. IV.

II. MODELS AND METHODS

A. Coupled quantum and classical Hamiltonians

The conduction electron subsystem is modeled by a quantum Hamiltonian

$$\mathbf{H}(t) = -\gamma\sum_{\langle ij\rangle}\hat{c}_i^\dagger\hat{c}_j - J_{\rm sd}\sum_i\hat{c}_i^\dagger\boldsymbol{\sigma}\cdot\mathbf{M}_i(t)\hat{c}_i, \quad (4)$$

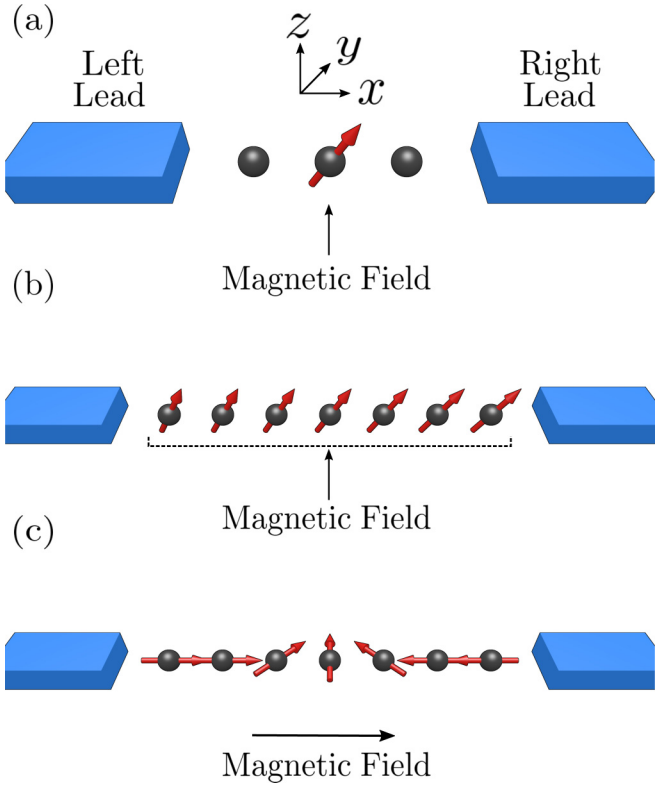

FIG. 1. Schematic view of two-terminal devices where an infinite 1D TB chain, describing electrons quantum mechanically, is attached to two macroscopic reservoirs while its middle part hosts: (a) single local magnetic moment, initially oriented in the $+x$ direction, placed in an external magnetic field pointing along the $+z$ direction; (b) 11 local magnetic moments (illustration shows 7 of them), initially oriented in the $+x$ direction, placed in an external magnetic field pointing along the $+z$ direction; (c) three-site-wide head-to-head magnetic DW whose motion is driven by an external magnetic field pointing in the $+x$ direction. Electrons within a 1D TB chain and classical local magnetic moments interact via the *s-d* exchange coupling of strength $J_{\rm sd}$, and classical local magnetic moments within the DW in (c) additionally interact with each other via the Heisenberg exchange coupling of strength J.

which is (assumed to be 1D for simplicity) a tight-binding (TB) model in which an electron interacts with magnetic moments localized at sites i, and it is described by the classical vector $\mathbf{M}_i(t)$ of unit length. Here $\hat{c}_i^\dagger = (\hat{c}_{i\uparrow}^\dagger, \hat{c}_{i\downarrow}^\dagger)$ is a row vector containing operators $\hat{c}_{i\sigma}^\dagger$ that create an electron of spin $\sigma = \uparrow, \downarrow$ at site i, $\hat{c}_i$ is a column vector that contains the corresponding annihilation operators, $\gamma = 1$ eV is the nearest-neighbor hopping, and $J_{\rm sd}$ is the *s-d* exchange coupling parameter between conduction electrons and local magnetic moments. The active region of devices depicted in Figs. 1(a)–1(c) consists of 1, 11, and 21 TB sites, respectively. These are attached to the left (L) and right (R) semi-infinite ideal leads modeled by the same Hamiltonian in Eq. (4) but with $J_{\rm sd} = 0$ eV. The leads are assumed to terminate into macroscopic reservoirs kept at the same chemical potential since we do not apply any bias voltage to the devices in Figs. 1(a)–1(c).

The classical Hamiltonian describing the local magnetic moments is given by

$$\mathcal{H} = -J\sum_{ij}\mathbf{M}_i\cdot\mathbf{M}_j - \mu_M\sum_i \mathbf{M}_i\cdot\mathbf{B}_{\rm ext}^i - K\sum_i\left(\mathrm{M}_i^x\right)^2 - J_{\rm sd}\sum_i\langle\hat{\mathbf{s}}\rangle^i\cdot\mathbf{M}_i, \tag{5}$$

where J is the Heisenberg exchange coupling parameter, $\mathbf{B}_{\rm ext}^i$ is the applied external magnetic field, K is the magnetic anisotropy (in the x direction), μ_M is the magnitude of the local magnetic moment [5], and $\langle\hat{\mathbf{s}}\rangle^i$ is the nonequilibrium electronic spin density computed from Eq. (3).

B. Time-retarded damping and magnetic inertia in the LLG equation self-consistently coupled to TDNEGF

The quantum equation of motion for the nonequilibrium density matrix of electrons [57,58]

$$i\hbar\frac{\partial\boldsymbol{\rho}_{\rm neq}(t)}{\partial t} = [\mathbf{H}(t), \boldsymbol{\rho}_{\rm neq}(t)] + \sum_{p=\mathrm{L,R}} i[\boldsymbol{\Pi}_p(t) + \boldsymbol{\Pi}_p^\dagger(t)] \tag{6}$$

is an example of a master equation for an open (i.e., connected to macroscopic reservoirs) quantum system [59] due to the presence of the second term on the right-hand side, in addition to standard terms of the von Neumann equation. This term and the density matrix itself can be expressed using the TDNEGF formalism [51,52] as

$$\boldsymbol{\rho}_{\rm neq}(t) = \frac{1}{i}\mathbf{G}^<(t,t')|_{t=t'}, \tag{7}$$

$$\boldsymbol{\Pi}_p(t') = \int_{-\infty}^{t'} dt_1[\mathbf{G}^>(t',t_1)\boldsymbol{\Sigma}_p^<(t_1,t') - \mathbf{G}^<(t',t_1)\boldsymbol{\Sigma}_p^>(t_1,t')]. \tag{8}$$

The central quantities of the TDNEGF formalism are the retarded $G_{ii'}^{r,\sigma\sigma'}(t,t') = -i\Theta(t-t')\langle\{\hat{c}_{i\sigma}(t), \hat{c}_{i'\sigma'}(t)\}\rangle$ and the lesser $G_{ii'}^{<,\sigma\sigma'}(t,t') = i\langle\hat{c}_{i'\sigma'}^\dagger(t')\hat{c}_{i\sigma}(t)\rangle$ Green functions (GFs), which describe the available density of states and how electrons occupy those states, respectively. In addition, it is also useful to introduce the greater GF, $\mathbf{G}^>(t,t') = [\mathbf{G}^<(t',t)]^\dagger$, and the advanced GF, $\mathbf{G}^a(t,t') = [\mathbf{G}^r(t,t')]^\dagger$. The current matrices $\boldsymbol{\Pi}_p(t)$ make it possible to compute directly [57,58] the charge current

$$I_p(t) = \frac{e}{\hbar}\mathrm{Tr}[\boldsymbol{\Pi}_p(t)], \tag{9}$$

and the spin current

$$I_p^{S_\alpha}(t) = \frac{e}{\hbar}\mathrm{Tr}[\hat{\sigma}^\alpha\boldsymbol{\Pi}_p(t)], \tag{10}$$

in the L and R semi-infinite leads. The equation of motion for the lesser and greater GFs is given by

$$i\hbar\frac{\partial\mathbf{G}^{>,<}(t,t_1)}{\partial t} = \mathbf{H}(t)\mathbf{G}^{>,<}(t,t_1) + \int_{-\infty}^{+\infty} dt_2\big[\boldsymbol{\Sigma}_{\rm tot}^r(t,t_2)\mathbf{G}^{>,<}(t_2,t) + \boldsymbol{\Sigma}_{\rm tot}^{>,<}(t,t_2)\mathbf{G}^a(t_2,t)\big], \tag{11}$$

where $\mathbf{\Sigma}^{r,>,<}_{\rm tot}(t,t_2)=\sum_{p=\rm L,R}\mathbf{\Sigma}^{r,>,<}_{p}(t,t_2)$ and $\mathbf{\Sigma}^{r,>,<}_{p}(t,t_2)$ are the lead self-energy matrices [52,57,58].

The classical equation of motion for the magnetic moment localized at site i is the Landau-Lifshitz equation

$$\frac{\partial \mathbf{M}_i(t)}{\partial t}=-g\mathbf{M}_i(t)\times\mathbf{B}^{\rm eff}_i(t), \tag{12}$$

where the effective magnetic field is $\mathbf{B}^{\rm eff}_i(t)=-\frac{1}{\mu_M}\partial\mathcal{H}/\partial\mathbf{M}_i$.

The full TDNEGF+LLG framework [50], which we also denote as TDNEGF$\leftrightarrows$LLG, consists of a self-consistent combination of Eqs. (6) and (12) where one first solves for the nonequilibrium electronic spin density in Eq. (3), which is then fed into Eq. (12) to propagate local magnetic moments $\mathbf{M}_i(t)$ in the next time step. Evolving $\boldsymbol{\rho}_{\rm neq}(t)$ via Eq. (6) requires a time step $\delta t=0.01$ fs for numerical stability, and we use the same time step to evolve LLG or Landau-Lifshitz equations for $\mathbf{M}_i(t)$. These updated local magnetic moments are fed back into the quantum Hamiltonian of the conduction electron subsystem in Eq. (4). Thus the obtained solutions for $\mathbf{M}_i(t)$, $\langle\hat{\mathbf{s}}\rangle^i(t)$, $I_p(t)$, and $I^{S_\alpha}_p(t)$ are numerically exact. For testing the importance of the self-consistent feedback loop, we also use TDNEGF$\leftarrow$LLG, where TDNEGF is utilized to obtain $I_p(t)$ and $I^{S_\alpha}_p(t)$ while the local magnetic moments are evolved solely by the conventional LLG Eq. (1), i.e., by using $J_{\rm sd}\equiv 0$ in Eq. (5) but $J_{\rm sd}\neq 0$ in Eq. (4).

In the weak-coupling limit [34,60] (i.e., small $J_{\rm sd}$) for electron-spin/local-magnetic-moment interaction it is possible to extract explicitly the generalized LLG equation with a memory kernel. For this purpose, we use the following expansions in the powers of small $J_{\rm sd}$:

$$\boldsymbol{\rho}_{\rm neq}(t)=\sum_{n=0}^{\infty}\boldsymbol{\rho}_n(t)J^n_{\rm sd}, \tag{13}$$

$$\mathbf{\Pi}_p(t')=\sum_{n=0}^{\infty}\mathbf{\Pi}^{(n)}_p(t')J^n_{\rm sd}, \tag{14}$$

$$\mathbf{G}^{r,a,>,<}(t',t_1)=\sum_{n=0}^{\infty}\mathbf{G}^{r,a,>,<}_n(t',t_1)J^n_{\rm sd}. \tag{15}$$

In Appendix, we show how to combine Eqs. (6), (11), (13), (14), and (15) to obtain the perturbative equation

$$\frac{\partial \mathbf{M}_i(t)}{\partial t}=-g\Bigg[\mathbf{M}_i(t)\times\mathbf{B}^{\rm eff,0}_i(t)+\frac{J^2_{\rm sd}}{\mu_M}\sum_{p=\rm L,R}\mathbf{M}_i(t)\times\int_{-\infty}^{+\infty}dt''\mathbf{M}_i(t'')\big\{\mathrm{K}^p_i(t'',t)+\mathrm{K}^{p*}_i(t'',t)\big\}\Bigg], \tag{16}$$

for the dynamics of each local magnetic moment at site i, by retaining only the terms linear in $J_{\rm sd}$ in Eqs. (13)–(15). Here $\mathbf{B}^{\rm eff,0}_i\equiv-\frac{1}{\mu_M}\partial\mathcal{H}^0/\partial\mathbf{M}_i$, $\mathcal{H}^0$ is the classical Hamiltonian in Eq. (5) with $J_{\rm sd}\equiv 0$, and $\mathrm{K}^p_i(t'',t)$ is defined in Appendix. The physical origin [35] of time-retardation effects described by the second term in Eq. (16) is that even though the electron dynamics is much faster than the dynamics of local magnetic moments, the nonequilibrium spin density in Eq. (3) is always behind $\mathbf{M}_i(t)$ and, therefore, is never parallel to it, which introduces the spin torque term into the Landau-Lifshitz Eq. (12). In other words, it takes a finite amount of time for conduction electron spin to react to the motion of classical local magnetic moments, so that nonequilibrium electrons effectively mediate interaction of $\mathbf{M}_i(t)$ with the same local magnetic moment at an earlier time $t'<t$. In the full TDNEGF+LLG scheme, such retardation effects are mediated by the nonequilibrium electrons starting at site i at time t' and returning back to the same site at time $t>t'$, while in the perturbative limit the same effect is captured by the second term in Eq. (16). The perturbative formula Eq. (16) is expected [35] to break down after propagation over time $t\sim\hbar/J_{\rm sd}$.

Further approximation to Eq. (16) can be made by considering sufficiently slow dynamics of local magnetic moments so that higher-order terms in the Taylor series,

$$\mathbf{M}_i(t'')\approx\mathbf{M}_i(t)+\frac{\partial\mathbf{M}_i(t)}{\partial t}(t''-t)+\frac{1}{2}\frac{\partial^2\mathbf{M}_i(t)}{\partial t^2}(t''-t)^2+\cdots, \tag{17}$$

can be neglected. By defining the following quantities:

$$\lambda^{\rm D}_{p,i}(t)\equiv\int_{-\infty}^{+\infty}dt''(t''-t)\big[\mathrm{K}^p_i(t'',t)+\mathrm{K}^{*p}_i(t'',t)\big] \tag{18}$$

and

$$I^{\rm D}_{p,i}(t)\equiv\frac{1}{2}\int_{-\infty}^{+\infty}dt''(t''-t)^2\big[\mathrm{K}^p_i(t'',t)+\mathrm{K}^{*p}_i(t'',t)\big], \tag{19}$$

and by retaining terms up to second order in Eq. (17), we obtain the conventionally looking LLG equation

$$\frac{\partial \mathbf{M}_i(t)}{\partial t}=-g\Bigg[\mathbf{M}_i(t)\times\mathbf{B}^{\rm eff,0}_i(t)+\frac{J^2_{\rm sd}}{\mu_M}\Bigg\{\sum_{p=\rm L,R}\lambda^{\rm D}_{p,i}(t)\Bigg\}\mathbf{M}_i(t)\times\frac{\partial\mathbf{M}_i(t)}{\partial t}+\frac{J^2_{\rm sd}}{\mu_M}\Bigg\{\sum_{p=\rm L,R}I^{\rm D}_{p,i}(t)\Bigg\}\mathbf{M}_i(t)\times\frac{\partial^2\mathbf{M}_i(t)}{\partial t^2}\Bigg]. \tag{20}$$

However, the Gilbert damping term prefactor

$$\lambda^{\rm D}_i(t)=-\frac{J^2_{\rm sd}}{\mu_M}\sum_{p=\rm L,R}\lambda^{\rm D}_{p,i}(t), \tag{21}$$

and the magnetic inertia term prefactor

$$I^{\rm D}_i(t)=-\frac{J^2_{\rm sd}}{\mu_M}\sum_{p=\rm L,R}I^{\rm D}_{p,i}(t), \tag{22}$$

in Eq. (20) are now time- and position-dependent. This is in sharp contrast to the conventional LLG Eq. (1) employed in classical micromagnetics where Gilbert damping and magnetic inertia prefactors are material-specific constants.

C. Comparison with static Gilbert damping from the scattering matrix approach

Static Gilbert damping caused by coupling of electrons to local magnetic moments in a two-terminal device [61] can also be calculated using the scattering matrix approach [62]. The LLG equation with nonlocal damping is given by

$$\frac{\partial \mathbf{M}_i(t)}{\partial t} = -g\mathbf{M}_i(t) \times \mathbf{B}_i^{\text{eff}}(t) + \sum_k \mathbf{M}_i(t) \times \hat{\mathrm{G}}_{ik} \frac{\partial \mathbf{M}_k(t)}{\partial t}, \tag{23}$$

where $\hat{\mathrm{G}}_{ik}$ is called the Gilbert damping tensor. One then introduces collective coordinates that are used to describe the dynamics of local magnetic moments, i.e., we make the assumption that there exist generalized coordinates $\boldsymbol{\xi}(t) \equiv [\xi_1(t), \xi_2(t), \ldots, \xi_N(t)]^{\mathrm{T}}$ such that $\mathbf{M}_i(t) = \mathbf{M}_i(\boldsymbol{\xi}(t))$. Then Eq. (23) can be recast into

$$\hat{\eta}\dot{\boldsymbol{\xi}} + \boldsymbol{\mathcal{F}} - \hat{\Gamma}\dot{\boldsymbol{\xi}} = 0, \tag{24}$$

where the elements of the matrices $\hat{\eta}$ and $\hat{\Gamma}$ are given by

$$(\hat{\eta})_{AB} \equiv \frac{\mu_M}{g} \sum_i \mathbf{M}_i \cdot \left(\frac{\partial \mathbf{M}_i}{\partial \xi_A} \times \frac{\partial \mathbf{M}_i}{\partial \xi_B} \right), \tag{25}$$

$$(\hat{\Gamma})_{AB} = \frac{\mu_M}{g} \sum_{ik} \left(\hat{\mathrm{G}}_{ik} \frac{\partial \mathbf{M}_k}{\partial \xi_A} \right) \cdot \left(\frac{\partial \mathbf{M}_i}{\partial \xi_B} \right), \tag{26}$$

respectively. The generalized force vector $\boldsymbol{\mathcal{F}}$ is given by

$$\boldsymbol{\mathcal{F}} = -\frac{\partial \mathcal{H}}{\partial \boldsymbol{\xi}}. \tag{27}$$

The scattering matrix approach allows us to compute $\hat{\Gamma}$ and $\boldsymbol{\mathcal{F}}$ as

$$(\hat{\Gamma})_{AB} = \frac{\hbar}{4\pi} \int dE \left(-\frac{\partial f}{\partial E} \right) \mathrm{Tr} \left[\frac{\partial \mathbf{S}(E)}{\partial \xi_A} \frac{\partial \mathbf{S}^\dagger(E)}{\partial \xi_B} \right], \tag{28}$$

$$\boldsymbol{\mathcal{F}} = -\frac{1}{2\pi i} \int dE\, f(E)\, \mathrm{Tr} \left[\mathbf{S}^\dagger(E) \frac{\partial \mathbf{S}(E)}{\partial \boldsymbol{\xi}} \right], \tag{29}$$

where $\mathbf{S}(E)$ is the scattering matrix of the device that is frozen at time t, while $f(E)$ is the Fermi function of the left and right reservoirs, which are held at an identical chemical potential.

For the case of a single local magnetic moment, the collective coordinates that describe the dynamics are given by the polar angle $\theta(t)$ and the azimuthal angle $\phi(t)$, so that $\mathbf{M}(t) = (\sin\theta\cos\phi, \sin\theta\sin\phi, \cos\theta)$. Furthermore, we can assume an isotropic system and, therefore, in Eq. (23) we have

$$G^{\alpha\beta} = \lambda_{\mathrm{S}} \delta^{\alpha\beta}, \tag{30}$$

where λ_{S} represents the static Gilbert damping. Using Eqs. (26) and (28), and assuming zero temperature, we obtain

$$\lambda_{\mathrm{S}} = \frac{g\hbar}{4\pi\mu_M} \mathrm{Tr} \left[\frac{\partial \mathbf{S}}{\partial \phi} \frac{\partial \mathbf{S}^\dagger}{\partial \phi} \right] \left(\frac{1}{\sin^2\theta} \right). \tag{31}$$

Equation (31) is evaluated for the case of a single local magnetic moment shown in Fig. 1(a) and plotted in Fig. 2(b).

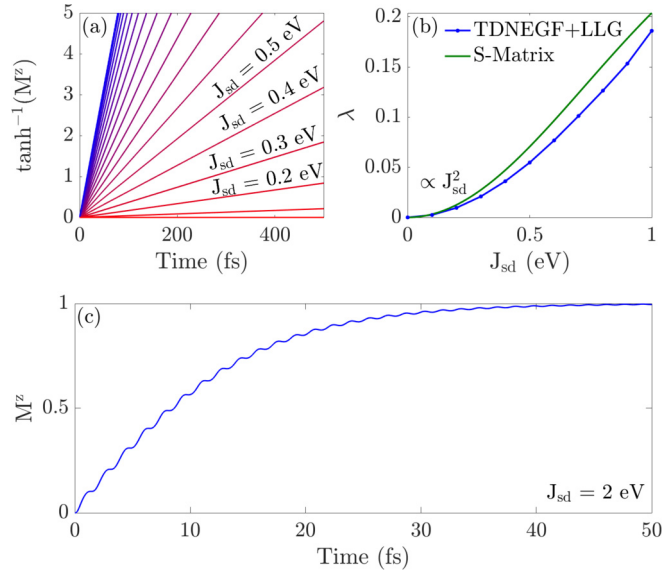

FIG. 2. (a) Time dependence of $\tanh^{-1}(M^z)$ for a single local magnetic moment in Fig. 1(a) obtained from TDNEGF+LLG simulations. Red to blue indicates increasing *s-d* exchange coupling in steps of 0.1 eV, ranging from $J_{\mathrm{sd}} = 0$ to 1.9 eV. (b) The dynamical Gilbert damping parameter in Eq. (21) (blue curve with circles) extracted from panel (a) as a function of J_{sd} and the Gilbert damping parameter obtained from the scattering (or S) matrix formula in Eq. (31) (solid green curve). (c) Time dependence of the M^z component for a single local magnetic moment in Fig. 1(a) at large $J_{\mathrm{sd}} = 2.0$ eV exhibits nutation as a signature of magnetic inertia. To generate fast magnetization dynamics and reduce simulation time, we use an unrealistically large external magnetic field of strength $B = 1000$ T. The conventional intrinsic Gilbert damping parameter is set to zero, $\lambda_{\mathrm{G}} = 0$, and the Fermi energy is $E_{\mathrm{F}} = 0$ eV.

III. RESULTS AND DISCUSSION

A. Single local magnetic moment in an external magnetic field

To compare the dynamics of local magnetic moments in full TDNEGF+LLG quantum-classical simulations versus conventional LLG classical simulations, we first consider a well-known example [5] for which the conventional LLG equation can be analytically solved—a single local magnetic moment that at $t = 0$ points along the $+x$ direction and then starts to precess due to an external magnetic field pointing in the $+z$ direction. Its trajectory is given by [5]

$$M^x(t) = \mathrm{sech}\left(\frac{g\lambda_{\mathrm{G}} B}{1+\lambda_{\mathrm{G}}^2} t \right) \cos\left(\frac{gB}{1+\lambda_{\mathrm{G}}^2} t \right), \tag{32a}$$

$$M^y(t) = \mathrm{sech}\left(\frac{g\lambda_{\mathrm{G}} B}{1+\lambda_{\mathrm{G}}^2} t \right) \sin\left(\frac{gB}{1+\lambda_{\mathrm{G}}^2} t \right), \tag{32b}$$

$$M^z(t) = \tanh\left(\frac{g\lambda_{\mathrm{G}} B}{1+\lambda_{\mathrm{G}}^2} t \right), \tag{32c}$$

where $\mathbf{B} = (0, 0, B)$ is the applied external magnetic field. Thus, if the conventional intrinsic Gilbert damping parameter is set to zero, $\lambda_{\mathrm{G}} = 0$, then the local magnetic moment precesses steadily around the z axis with $M^z \equiv 0$. On the other hand, for nonzero $\lambda_{\mathrm{G}} > 0$, the local magnetic moment will relax toward the direction of the magnetic

field, i.e., $\lim_{t\to\infty}(M^x(t), M^y(t), M^z(t)) = (0, 0, 1)$. Thus, such damped dynamics is signified by a linear $\tanh^{-1}(M^z)$ versus time dependence. Figure 2 plots the results of TDNEGF+LLG simulations for the same problem. Even though we set conventional intrinsic Gilbert damping to zero, $\lambda_G = 0$, Fig. 2(a) shows linear $\tanh^{-1}(M^z)$ versus time, independently of the strength of *s-d* exchange coupling as long as $J_{sd} \lesssim 2$ eV. This means that the local magnetic moment is experiencing (time-independent) dynamical Gilbert damping $\lambda^D \propto J_{sd}^2$, in accord with Eq. (21) and as shown in Fig. 2(b) (blue curve with circles), which is generated solely by the TDNEGF part of the self-consistent loop within the full TDNEGF+LLG scheme.

We also show in Fig. 2(b) that the Gilbert damping λ_S, calculated using the scattering matrix formula in Eq. (31), agrees well with our dynamical Gilbert damping in the limit of weak strength of *s-d* exchange coupling ($J_{sd} \lesssim 0.2$ eV). However, there is a disagreement between the two at larger strengths of *s-d* exchange coupling. We attribute this result to the fast dynamics of local magnetic moments, in which case the dynamics becomes nonadiabatic and the scattering matrix approach is no longer applicable. We also emphasize that our dynamical Gilbert damping will become time- and spatially dependent for more than one local magnetic moment studied in Sec. III B, so that it cannot be mimicked by a single time-independent parameter λ_S obtained from the scattering matrix formula in Eq. (31).

For $J_{sd} \gtrsim 2$ eV, the dynamics of the local magnetic moment also exhibits nutation [35], as shown in Fig. 2(c), which is the signature of the magnetic inertia [19–24] term $\propto \mathbf{M}_i \times \partial^2\mathbf{M}_i/\partial t^2$ in Eq. (20). Thus, nutation becomes conspicuous when the dynamics of the local magnetic moments is sufficiently fast, so that $\partial^2\mathbf{M}_i/\partial t^2$ is large, as well as when the interaction between the itinerant and localized spins is sufficiently large.

B. Multiple exchange-uncoupled local magnetic moments in an external magnetic field

To examine the possible spatial dependence of the dynamical Gilbert damping parameter or the emergence of dynamical exchange coupling [63,64] between local magnetic moments, we consider a chain of $N = 11$ magnetic moments that do not interact with each other ($J = 0$) but interact with conduction electron spin ($J_{sd} \neq 0$), as illustrated in Fig. 1(b). At $t = 0$, all magnetic moments point in the $+x$ direction while the external magnetic field is in the $+z$ direction, and the conventional intrinsic Gilbert damping is set to zero, $\lambda_G = 0$.

Figures 3(a) and 3(c) show the trajectory of selected local magnetic moments ($i = 1$ and 6) on the Bloch sphere for $J_{sd} = 0.1$ eV. In contrast to the single local magnetic moment in Fig. 2(a), for which $\tanh^{-1}(M^z)$ versus time is linear using $J_{sd} = 0.1$ eV, we find that in the case of multiple exchange-uncoupled magnetic moments this is no longer the case, as demonstrated by Figs. 3(b) and 3(d). Hence, the trajectory followed by these local magnetic moments cannot be described by Eq. (32) so that the conventional-like Gilbert damping parameter cannot be extracted anymore. Thus, such a nonstandard damping of the dynamics of local magnetic moments originates from the time dependence of the dynamical damping parameter λ_i^D in Eq. (21).

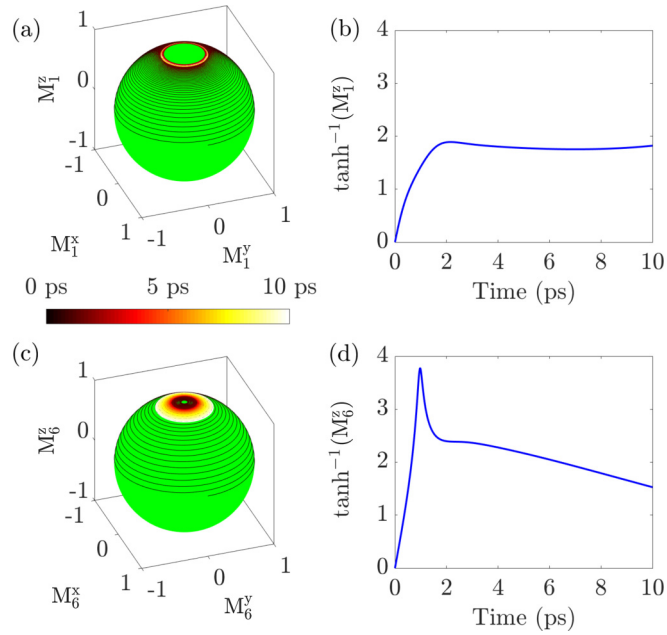

FIG. 3. TDNEGF+LLG-computed trajectories $(M^x(t), M^y(t), M^z(t))$ on the Bloch sphere of local magnetic moment in the setup of Fig. 1(b) at (a) site 1 and (c) site 6. The total number of local magnetic moments is $N = 11$, and they do not interact with each other via exchange coupling [i.e., $J = 0$ eV in Eq. (5)]. Panels (b) and (d) show the corresponding time dependence of the M^z component from panels (a) and (c), respectively. The external magnetic field is $B = 1000$ T, and the *s-d* exchange coupling strength $J_{sd} = 0.1$ eV is *nonperturbative* in this setup, therefore it does *not* allow us to extract explicitly the dynamical Gilbert damping parameter from Eq. (21). The conventional intrinsic Gilbert damping parameter is set to zero, $\lambda_G = 0$, and the Fermi energy is $E_F = 0$ eV.

Figure 4(a) shows $\tanh^{-1}(M^z)$ versus time for selected local magnetic moments ($i = 1$, 3, and 6) and smaller $J_{sd} =$

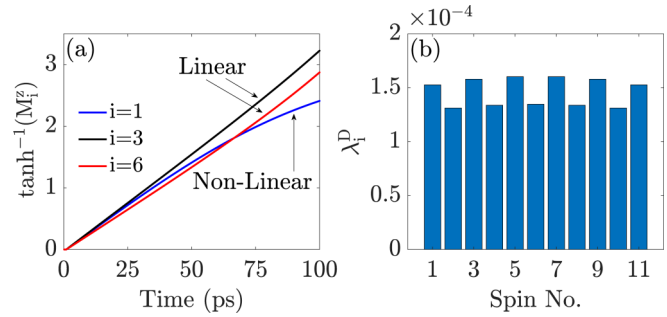

FIG. 4. (a) TDNEGF+LLG-computed time dependence of the M^z component of the local magnetic moment on sites 1, 3, and 6 in the setup of Fig. 1(b) with a total of $N = 11$ moments. (b) Position dependence of the dynamical Gilbert damping parameter in Eq. (21). The external magnetic field is $B = 1000$ T, and the *s-d* exchange coupling strength $J_{sd} = 0.01$ eV is *perturbative* in this setup, therefore it allows us to extract the dynamical Gilbert damping explicitly from Eq. (21). The conventional intrinsic Gilbert damping parameter is set to zero, $\lambda_G = 0$, and the Fermi energy is $E_F = 0$ eV.

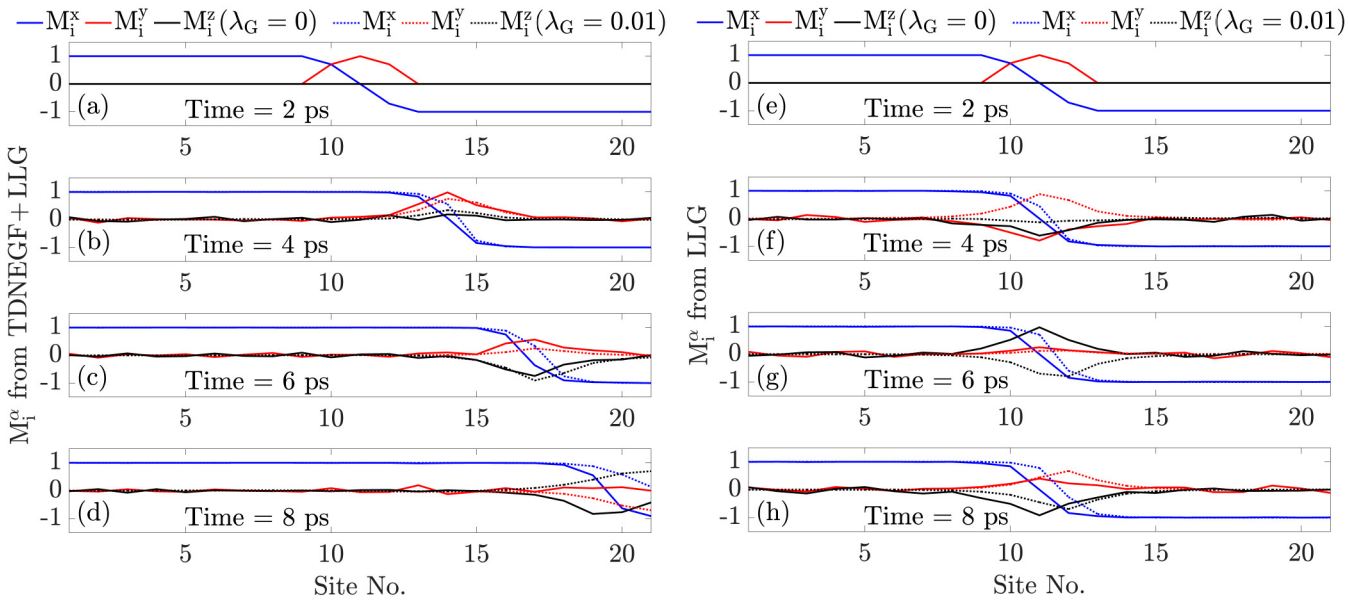

FIG. 5. (a)–(d) TDNEGF+LLG-computed snapshots of head-to-head DW in the setup of Fig. 1(c) driven by an external magnetic field of strength $B = 100$ T pointing in the $+x$ direction, in the absence ($\lambda_G = 0$) or presence ($\lambda_G = 0.01$) of conventional intrinsic Gilbert damping. Panels (e)–(h) show the corresponding snapshots computed solely by the conventional LLG Eq. (1) where in the absence ($\lambda_G = 0$) of conventional intrinsic Gilbert damping the DW does not move at all. The Heisenberg exchange coupling between local magnetic moments is $J = 0.01$ eV, s-d exchange coupling between electrons and local magnetic moments is $J_{sd} = 0.1$ eV, magnetic anisotropy (in the x direction) is $K = 0.01$ eV, and the Fermi energy of electrons is $E_F = -1.9$ eV. The magnetic field is applied at $t = 2$ ps, while prior to that we evolve the conduction electron subsystem with TDNEGF until it reaches thermodynamic equilibrium, where all transient spin and charge currents have decayed to zero.

0.01 eV. Although all local magnetic moments follow linear $\tanh^{-1}(M^z)$ versus time, as predicted by the solution in Eq. (32c) of the conventional LLG equation, the dynamical Gilbert damping extracted from Eq. (32) changes from site to site as shown in Fig. 4(b). Furthermore, the linear $\tanh^{-1}(M^z)$ versus time relation breaks down for times $t \gtrsim 50$ ps at specific sites, which then prevents extracting time-independent λ_i^D at those sites.

C. Magnetic field-driven motion of a domain wall composed of multiple exchange-coupled local magnetic moments

To examine the difference in the predicted dynamics of exchange-coupled local magnetic moments by the TDNEGF+LLG framework versus the conventional LLG equation, we consider the simplest example of the 1D head-to-head magnetic DW depicted in Fig. 1(c). Its motion is driven by applying an external magnetic field in the $+x$ direction. Some type of damping mechanism is crucial for the DW to move, as demonstrated by the solid lines in Figs. 5(e)–5(h), obtained by solving the conventional LLG equation with $\lambda_G = 0$, which show how local magnetic moments precess around the magnetic field but without net displacement of the center of the DW.

On the other hand, even though we set $\lambda_G = 0$ in TDNEGF+LLG simulations in Figs. 5(a)–5(d), the center of the DW moves to the right due to dynamically generated time-retarded damping encoded by the memory kernel in Eq. (16). Including the conventional intrinsic Gilbert damping, $\lambda_G = 0.01$, as is often used in micromagnetic simulations of DW along magnetic nanowires [43,44,65], changes only slightly the result of TDNEGF+LLG simulations, which demonstrates that the effective dynamical Gilbert damping (which is also time-dependent) is about an order of magnitude larger than λ_G. This is also reflected in the DW velocity being much larger in TDNEGF+LLG simulations with $\lambda_G = 0$ in Figs. 5(a)–5(d) than in the conventional LLG equation simulations with $\lambda_G = 0.01$ in Figs. 5(e)–5(h).

It has been predicted theoretically [12,53,66–70] and confirmed experimentally [71] that a moving DW will pump charge current even in the absence of any applied bias voltage. The corresponding open circuit pumping voltage in the so-called spin motive force (SMF) theory [12,53] is given by

$$V_{\rm SMF} = \frac{1}{G_0}\int j_x dx, \tag{33a}$$

$$j_\alpha(\mathbf{r}) = \frac{P\sigma_0\hbar}{2e}[\partial_t \mathbf{m}(\mathbf{r},t)\times\partial_\alpha \mathbf{m}(\mathbf{r},t)]\cdot\mathbf{m}(\mathbf{r},t), \tag{33b}$$

where j_x is the pumped local charge current along the x axis. Here $\sigma_0 = \sigma^\uparrow + \sigma^\downarrow$ is the total conductivity, $P = (\sigma^\uparrow - \sigma^\downarrow)/(\sigma^\uparrow + \sigma^\downarrow)$ is the spin polarization of the ferromagnet, and $\partial_t = \partial/\partial t$. Equation (33) is typically combined [54–56] with classical micromagnetics, which supplies $\mathbf{M}_i(t)$, which is then plugged into the discretized version [50]

$$j_x(i) \propto \frac{1}{a}\{\partial_t \mathbf{M}_i(t)\times[\mathbf{M}_{i+1}(t) - \mathbf{M}_i(t)]\}\cdot\mathbf{M}_i(t)$$
$$\propto \frac{1}{a}[\partial_t \mathbf{M}_i(t)\times\mathbf{M}_{i+1}(t)]\cdot\mathbf{M}_i(t) \tag{34}$$

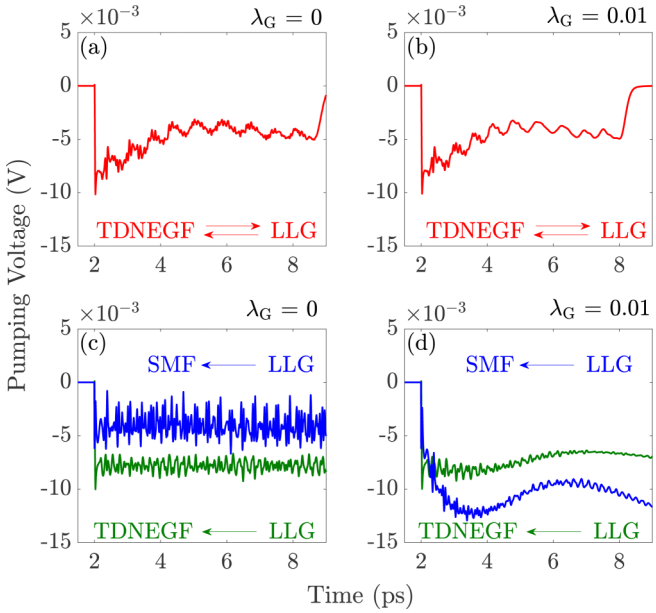

FIG. 6. Time dependence of pumping voltage generated by the DW motion depicted in Figs. 5(a)–5(d) for (a) $\lambda_G = 0$ and (b) $\lambda_G = 0.01$. In panels (a) and (b), local magnetic moments evolve in time by the full TDNEGF+LLG framework where the arrows indicate how TDNEGF sends nonequilibrium electronic spin density into the LLG equation, which in turn sends trajectories of local magnetic moments into TDNEGF. Time dependence of pumping voltage generated by DW motion depicted in Figs. 5(e)–5(h) for (c) $\lambda_G = 0$ and (d) $\lambda_G = 0.01$. In panels (c) and (d), local magnetic moments evolve in time using the conventional LLG equation, which sends their trajectories into either TDNEGF (green) or SMF formulas (blue) in Eq. (35) or Eq. (33), respectively, to obtain the corresponding pumping voltage.

of Eq. (33b). We denote this approach as SMF←LLG, which is perturbative in nature [69,72] since it considers only the lowest temporal and spatial derivatives.

On the other hand, the same pumping voltage can be computed nonperturbatively,

$$V_{\mathrm{TDNEGF}} = \frac{I_p(t)}{G(t)}, \tag{35}$$

using the TDNEGF expression for charge current in lead p in Eq. (9), where TDNEGF calculations are coupled to LLG calculations either self-consistently (i.e., by using TDNEGF⇆LLG) or non-self-consistently (i.e., by using TDNEGF←LLG). Here, $G(t)$ is the conductance computed using the Landauer formula applied to two-terminal devices with a frozen at time t texture of local magnetic moments.

Figures 6(a) and 6(b) plot the pumping voltage calculated by TDNEGF⇆LLG for DW motion shown in Figs. 5(a)–5(d) in the absence or presence of conventional Gilbert damping, respectively. The two cases are virtually identical due to an order of magnitude larger dynamical Gilbert damping that is automatically generated by TDNEGF⇆LLG in both Figs. 6(a) and 6(b). The nonperturbative results in Figs. 6(a) and 6(b) are quite different from SMF←LLG predictions in Figs. 6(c) and 6(d), respectively. This is due to both the failure of Eqs. (33) and (34) to describe noncoplanar and noncollinear magnetic textures with neighboring local magnetic moments tilted by more than 10° [50], and the lack of dynamical Gilbert damping in SMF←LLG simulations [54–56]. The latter effect is also emphasized by the inability of TDNEGF←LLG in Figs. 6(c) and 6(d) to reproduce the results of self-consistent TDNEGF⇆LLG in Figs. 6(a) and 6(b), respectively.

IV. CONCLUSIONS

In conclusion, we delineated a hierarchy of theoretical descriptions of a nonequilibrium quantum many-body system in which conduction electron spins interact with local magnetic moments within a ferromagnetic layer sandwiched between normal metal electrodes. On the top of the hierarchy is a fully quantum approach, for both electrons and local magnetic moments, whose computational complexity (using either original spin operators [73,74] for local magnetic moments, or their mapping to bosonic operators in order to enable application of many-body perturbation theory within the NEGF formalism [75]) makes it impractical for systems containing a large number of local magnetic moments. The next approach in the hierarchy is a computationally much less expensive quantum-classical hybrid [76] based on self-consistent coupling [50] of TDNEGF (which can be implemented using algorithms that scale linearly with both system size and simulation time [52,58,77]) with the classical LLG equation for local magnetic moments. Such a TDNEGF+LLG approach is numerically exact and, therefore, nonperturbative in the strength of electron-spin/local-magnetic-moment interaction, the speed of local magnetic moment dynamics, and the degree of noncollinearity between them. Even though electron dynamics is much faster than localized spin dynamics, the most general situation cannot be handled by integrating out [6,34] the conduction electron degrees of freedom and by focusing only on the LLG-type equation where a much larger time step can be used to propagate spins only.

Nevertheless, in the limit [34,60] of weak electron-spin/local-magnetic-moment interaction [i.e., small J_{sd} in Eqs. (4) and (5)], one can derive analytically a type of generalized LLG equation [34–37] for each local magnetic moment, which is the next approach in the hierarchy that sheds light on different effects included in the numerically exact TDNEGF+LLG scheme. Instead of the conventional Gilbert damping term in Eq. (1), the generalized LLG equation we derive as Eq. (16) contains a microscopically determined memory kernel that describes time-retardation effects generated by the coupling to TDNEGF. Fundamentally, the memory kernel is due to the fact that electron spin can never follow instantaneously a change in the orientation of the local magnetic moments [35]. In the limit of slow dynamics of local magnetic moments, one can further expand the memory kernel into a Taylor series to obtain the final approach within the hierarchy whose LLG Eq. (20) is akin to the conventional one, but which contains both Gilbert damping (proportional to the first time derivative of local magnetization) and magnetic inertia terms (proportional to the second time derivative of local magnetization) with *time-dependent* parameters instead of the usually assumed materials-specific constants.

Using three simple examples—single or multiple local magnetic moments precessing in an external magnetic field,

or magnetic-field-driven magnetic DW motion—we demonstrate the importance of dynamically induced damping, which operates even if conventional static Gilbert damping is set to zero. We also show that our dynamical Gilbert damping is approximately equal to the Gilbert damping predicted by the adiabatic S-matrix theory for weak electron-spin/local-magnetic-moment interaction. In the case of field-driven magnetic DW motion, we can estimate that the strength of dynamical damping is effectively *an order of magnitude larger* than the typically assumed [43,44,65] conventional static Gilbert damping $\lambda_G \simeq 0.01$ in classical micromagnetic simulations of magnetic nanowires. In addition, we show that charge pumping by the dynamics of noncoplanar and noncollinear magnetic textures, which is outside of the scope of pure micromagnetic simulations but is often described by combining [54–56] them with the SMF theory formula [12,53], requires us to take into account both the dynamical Gilbert damping and possibly the large angle between neighboring local magnetic moments in order to reproduce numerically exact results of the TDNEGF+LLG scheme.

ACKNOWLEDGMENTS

We thank Z. Yuan for insightful discussions. This work was supported by NSF Grant No. CHE 1566074. The supercomputing time is provided by XSEDE, which is supported by NSF Grant No. ACI-1548562.

APPENDIX: DERIVATION OF THE MEMORY KERNEL IN THE LLG EQUATION SELF-CONSISTENTLY COUPLED TO TDNEGF

In this Appendix, we provide a detailed derivation of the memory kernel in Eq. (16). To obtain the perturbative equation of motion for local magnetic moments, we start from the Landau-Lifshitz Eq. (12) where the effective magnetic field can be written as

$$\mathbf{B}_i^{\rm eff}(t) = \mathbf{B}_i^{\rm eff,0}(t) + J_{\rm sd}\langle\hat{\mathbf{s}}\rangle^i(t). \tag{A1}$$

The nonequilibrium spin density is expanded up to terms linear in $J_{\rm sd}$ using Eq. (13),

$$\begin{aligned}\langle\hat{\mathbf{s}}\rangle^i(t) &= \frac{\hbar}{2}\,{\rm Tr}[\boldsymbol{\rho}_{\rm neq}(t)\,|i\rangle\,\langle i|\otimes\boldsymbol{\sigma}] - \langle\hat{\mathbf{s}}\rangle^i_{\rm eq}\\ &\approx \frac{\hbar}{2}\,{\rm Tr}[\{\boldsymbol{\rho}_0(t) + J_{\rm sd}\boldsymbol{\rho}_1(t)\}\,|i\rangle\,\langle i|\otimes\boldsymbol{\sigma}] - \langle\hat{\mathbf{s}}\rangle^i_{\rm eq}\\ &= J_{\rm sd}\frac{\hbar}{2}\,{\rm Tr}[\boldsymbol{\rho}_1(t)\,|i\rangle\,\langle i|\otimes\boldsymbol{\sigma}] - \langle\hat{\mathbf{s}}\rangle^i_{\rm eq}.\end{aligned} \tag{A2}$$

Here $\langle\hat{\mathbf{s}}\rangle^i_{\rm eq}$ is the equilibrium electronic spin density, i.e., $\langle\hat{\mathbf{s}}\rangle^i_{\rm eq} = (\hbar/2)\,{\rm Tr}\,[\boldsymbol{\rho}_{\rm eq}\,|i\rangle\,\langle i|\otimes\boldsymbol{\sigma}]$. Furthermore, the electronic spin density in zeroth order must vanish, i.e., ${\rm Tr}\,[\boldsymbol{\rho}_0(t)\,|i\rangle\,\langle i|\otimes\boldsymbol{\sigma}] = 0$, since for $J_{\rm sd} = 0$ electrons are not spin-polarized. Hence, we can write Eq. (12) as

$$\begin{aligned}\frac{\partial\mathbf{M}_i(t)}{\partial t} = -g\mathbf{M}_i(t)\times\Bigg[&\mathbf{B}_i^{\rm eff,0}(t) + J_{\rm sd}^2\frac{\hbar}{2}\,{\rm Tr}[\boldsymbol{\rho}_1(t)\,|i\rangle\,\langle i|\otimes\boldsymbol{\sigma}]\\ &- J_{\rm sd}\langle\hat{\mathbf{s}}\rangle^i_{\rm eq}\Bigg].\end{aligned} \tag{A3}$$

To obtain analytical results, we assume that the equilibrium spin density follows the direction of local magnetic moments, so that $\mathbf{M}_i(t)\times\langle\hat{\mathbf{s}}\rangle^i_{\rm eq} = 0$. By expanding Eq. (6) we obtain

$$i\hbar\frac{\partial\boldsymbol{\rho}_0(t)}{\partial t} = [\mathbf{H}_0(t),\boldsymbol{\rho}_0(t)] + \sum_{p={\rm L,R}} i\big[\boldsymbol{\Pi}_p^{(0)}(t) + \boldsymbol{\Pi}_p^{(0)\dagger}(t)\big] \tag{A4}$$

and

$$i\hbar\frac{\partial\boldsymbol{\rho}_1(t)}{\partial t} = [\mathbf{H}_1(t),\boldsymbol{\rho}_0(t)] + i\sum_{p={\rm L,R}}\big[\boldsymbol{\Pi}_p^{(1)}(t) + \boldsymbol{\Pi}_p^{(1)\dagger}(t)\big], \tag{A5}$$

where $\mathbf{H}_1(t) = -\sum_i |i\rangle\,\langle i|\otimes\boldsymbol{\sigma}\cdot\mathbf{M}_i(t)$. One can formally integrate Eq. (A5), which leads to

$$\begin{aligned}\frac{\hbar}{2}\,{\rm Tr}[\boldsymbol{\rho}_1(t)\,|i\rangle\,\langle i|\otimes\boldsymbol{\sigma}] = \sum_{p={\rm L,R}}\frac{1}{2}\int_{-\infty}^{t}dt'\,{\rm Tr}\big[\big\{&\boldsymbol{\Pi}_p^{(1)}(t')\\ &+\boldsymbol{\Pi}_p^{(1)\dagger}(t')\big\}\,|i\rangle\,\langle i|\otimes\boldsymbol{\sigma}\big],\end{aligned} \tag{A6}$$

which requires us to find an expression for $\boldsymbol{\Pi}_p^{(1)}(t')$. Using Eq. (8) and the fact that lead self-energy matrices do not depend on $J_{\rm sd}$ leads to

$$\begin{aligned}\boldsymbol{\Pi}_p^{(1)}(t') = \int_{-\infty}^{t'}dt_1[&\mathbf{G}_1^{>}(t',t_1)\boldsymbol{\Sigma}_p^{<}(t_1,t')\\ &-\mathbf{G}_1^{<}(t',t_1)\boldsymbol{\Sigma}_p^{>}(t_1,t')].\end{aligned} \tag{A7}$$

Equations (11) and (15) can be formally integrated to yield lesser and greater GFs in Eq. (A7),

$$\begin{aligned}\mathbf{G}_1^{>,<}(t',t_1) = \frac{1}{i\hbar}\Bigg(&\int_{-\infty}^{t'}dt''\mathbf{H}_1(t'')\mathbf{G}_0^{>,<}(t'',t_1)\\ &+\int_{-\infty}^{t'}dt''\int_{-\infty}^{+\infty}dt_2\big[\boldsymbol{\Sigma}_{\rm tot}^{r}(t'',t_2)\mathbf{G}_1^{>,<}(t_2,t'')\\ &+\boldsymbol{\Sigma}_{\rm tot}^{>,<}(t'',t_2)\mathbf{G}_1^{a}(t_2,t'')\big]\Bigg).\end{aligned} \tag{A8}$$

We further assume that the active region in Fig. 1 is weakly coupled with semi-infinite leads and, therefore, macroscopic reservoirs into which they terminate. This means that after we substitute Eq. (A8) into Eq. (A7) we can keep only those terms that are linear in the self-energy,

$$\begin{aligned}&\boldsymbol{\Pi}_p^{(1)}(t')\\ &= \frac{1}{2i}\int_{-\infty}^{t'}dt''\mathbf{H}_1(t'')\int_{-\infty}^{t'}dt_1[\mathbf{G}_0^{>}(t'',t_1)\boldsymbol{\Sigma}_p^{<}(t_1,t')\\ &\quad-\mathbf{G}_0^{<}(t'',t_1)\boldsymbol{\Sigma}_p^{>}(t_1,t')]\end{aligned} \tag{A9}$$

$$\begin{aligned}&= \frac{i}{2}\sum_i\int_{-\infty}^{t'}dt''\,|i\rangle\,\langle i|\otimes\boldsymbol{\sigma}\cdot\mathbf{M}_i(t'')\\ &\quad\times\int_{-\infty}^{t'}dt_1[\mathbf{G}_0^{>}(t'',t_1)\boldsymbol{\Sigma}_p^{<}(t_1,t') - \mathbf{G}_0^{<}(t'',t_1)\boldsymbol{\Sigma}_p^{>}(t_1,t')]\end{aligned} \tag{A10}$$

$$= i\sum_i\int_{-\infty}^{t'}dt''\,|i\rangle\,\langle i|\otimes\boldsymbol{\sigma}\cdot\mathbf{M}_i(t'')\mathbf{A}_p^0(t'',t'), \tag{A11}$$

where $\mathbf{A}_p^0(t'',t')$ is an operator constructed out of the zeroth-order terms in the expansion of GFs shown in Eq. (15),

$$\mathbf{A}_p^0(t'',t') \equiv \frac{i}{2}\int_{-\infty}^{t'} dt_1 \Big[\mathbf{G}_0^{>}(t'',t_1)\boldsymbol{\Sigma}_p^{<}(t_1,t') - \mathbf{G}_0^{<}(t'',t_1)\boldsymbol{\Sigma}_p^{>}(t_1,t')\Big]. \tag{A12}$$

By plugging in Eqs. (A11) and (A12) into Eq. (A6), we obtain

$$\frac{\hbar}{2}\,\mathrm{Tr}[\boldsymbol{\rho}_1(t)\,|i\rangle\,\langle i|\otimes\hat{\sigma}^{\mu}] = \sum_{p=\mathrm{L,R}}\sum_{j}\sum_{\nu}\int_{-\infty}^{t} dt'\int_{-\infty}^{t'} dt''\mathrm{M}_j^{\nu}(t'')\,\mathrm{Tr}\big[\,|j\rangle\,\langle j| \otimes\hat{\sigma}^{\nu}\big\{\mathbf{A}_p^0(t'',t')+\mathbf{A}_p^{0\dagger}(t'',t')\big\}\,|i\rangle\,\langle i|\otimes\sigma^{\mu}\big]. \tag{A13}$$

Since $\mathbf{A}_p^0(t'',t')$ is an operator constructed from the zeroth-order GFs, it can be written in the following form:

$$\mathbf{A}_p^0(t'',t') = \frac{1}{2}\sum_{mn}\mathrm{A}_{mn}^{p}(t'',t')|m\rangle\langle n|\otimes 1_2, \tag{A14}$$

where 1_2 is a 2×2 identity matrix. Using this, it is easy to show that

$$\frac{\hbar}{2}\,\mathrm{Tr}[\boldsymbol{\rho}_1(t)\,|i\rangle\,\langle i|\otimes\boldsymbol{\sigma}] = \sum_{p=\mathrm{L,R}}\int_{-\infty}^{+\infty}\Theta(t-t')dt' \times\int_{-\infty}^{+\infty} dt''\mathbf{M}_i(t'')\big\{\mathrm{A}_{ii}^{p}(t'',t') + \mathrm{A}_{ii}^{p*}(t'',t')\big\}\Theta(t'-t'') \tag{A15}$$

and

$$\mathrm{K}_i^{p}(t'',t) = \int_{-\infty}^{+\infty} dt'\Theta(t-t')\Theta(t'-t'')\mathrm{A}_{ii}^{p}(t'',t'). \tag{A16}$$

By plugging in Eq. (A15) into the second term on the right-hand side of Eq. (A3), we finally obtain Eq. (16) of the main text.

[1] G. Bertotti, I. D. Mayergoyz, and C. Serpico, *Nonlinear Magnetization Dynamics in Nanosystems* (Elsevier, Amsterdam, 2009).
[2] R. Wieser, Phys. Rev. Lett. **110**, 147201 (2013).
[3] R. Wieser, Eur. Phys. J. B **88**, 77 (2015).
[4] D. Kumar and A. O. Adeyeye, J. Phys. D **50**, 343001 (2017).
[5] R. F. L. Evans, W. J. Fan, P. Chureemart, T. A. Ostler, M. O. A. Ellis, and R. W. Chantrell, J. Phys.: Condens. Matter **26**, 103202 (2014).
[6] A. S. Núñez and R. A. Duine, Phys. Rev. B **77**, 054401 (2008).
[7] V. Kamberský, Phys. Rev. B **76**, 134416 (2007).
[8] K. Gilmore, Y. U. Idzerda, and M. D. Stiles, Phys. Rev. Lett. **99**, 027204 (2007).
[9] F. Mahfouzi, J. Kim, and N. Kioussis, Phys. Rev. B **96**, 214421 (2017).
[10] D. Ralph and M. Stiles, J. Magn. Magn. Mater. **320**, 1190 (2008).
[11] Y. Tserkovnyak, A. Brataas, G. E. W. Bauer, and B. I. Halperin, Rev. Mod. Phys. **77**, 1375 (2005).
[12] S. Zhang and S. S.-L. Zhang, Phys. Rev. Lett. **102**, 086601 (2009).
[13] C. H. Wong and Y. Tserkovnyak, Phys. Rev. B **80**, 184411 (2009).
[14] Y. Tserkovnyak, E. M. Hankiewicz, and G. Vignale, Phys. Rev. B **79**, 094415 (2009).
[15] K.-W. Kim, J.-H. Moon, K.-J. Lee, and H.-W. Lee, Phys. Rev. Lett. **108**, 217202 (2012).
[16] H. T. Nembach, J. M. Shaw, C. T. Boone, and T. J. Silva, Phys. Rev. Lett. **110**, 117201 (2013).
[17] T. Weindler, H. G. Bauer, R. Islinger, B. Boehm, J.-Y. Chauleau, and C. H. Back, Phys. Rev. Lett. **113**, 237204 (2014).
[18] Y. Li and W. E. Bailey, Phys. Rev. Lett. **116**, 117602 (2016).
[19] M. Fähnle, D. Steiauf, and C. Illg, Phys. Rev. B **84**, 172403 (2011).
[20] S. Bhattacharjee, L. Nordström, and J. Fransson, Phys. Rev. Lett. **108**, 057204 (2012).
[21] T. Kikuchi and G. Tatara, Phys. Rev. B **92**, 184410 (2015).
[22] M. Sayad, R. Rausch, and M. Potthoff, Europhys. Lett. **116**, 17001 (2016).
[23] R. Mondal, M. Berritta, A. K. Nandy, and P. M. Oppeneer, Phys. Rev. B **96**, 024425 (2017).
[24] R. Mondal, M. Berritta, and P. M. Oppeneer, J. Phys.: Condens. Matter **30**, 265801 (2018).
[25] Y. Li, A.-L. Barra, S. Auffret, U. Ebels, and W. E. Bailey, Phys. Rev. B **92**, 140413 (2015).
[26] K. Carva and I. Turek, Phys. Rev. B **76**, 104409 (2007).
[27] Y. Liu, Z. Yuan, R. J. H. Wesselink, A. A. Starikov, and P. J. Kelly, Phys. Rev. Lett. **113**, 207202 (2014).
[28] S. Wang, Y. Xu, and K. Xia, Phys. Rev. B **77**, 184430 (2008).
[29] M. O. A. Ellis, M. Stamenova, and S. Sanvito, Phys. Rev. B **96**, 224410 (2017).
[30] B. K. Nikolić, K. Dolui, M. Petrović, P. Plecháč, T. Markussen, and K. Stokbro, in *Handbook of Materials Modeling*, edited by W. Andreoni and S. Yip (Springer, Cham, 2019), pp. 1–35.
[31] D. Thonig, O. Eriksson, and M. Pereiro, Sci. Rep. **7**, 931 (2017).
[32] T. Bose and S. Trimper, Phys. Rev. B **83**, 134434 (2011).
[33] D. Thonig, J. Henk, and O. Eriksson, Phys. Rev. B **92**, 104403 (2015).
[34] M. Onoda and N. Nagaosa, Phys. Rev. Lett. **96**, 066603 (2006).
[35] M. Sayad and M. Potthoff, New J. Phys. **17**, 113058 (2015).
[36] H. Hammar and J. Fransson, Phys. Rev. B **94**, 054311 (2016).
[37] H. Hammar and J. Fransson, Phys. Rev. B **96**, 214401 (2017).
[38] P. He, X. Ma, J. W. Zhang, H. B. Zhao, G. Lüpke, Z. Shi, and S. M. Zhou, Phys. Rev. Lett. **110**, 077203 (2013).
[39] K. J. Lee, A. Deac, O. Redon, J. P. Nozières, and B. Dieny, Nat. Mater. **3**, 877 (2004).
[40] M. D. Stiles, W. M. Saslow, M. J. Donahue, and A. Zangwill, Phys. Rev. B **75**, 214423 (2007).

[41] Z. Li and S. Zhang, Phys. Rev. B **70**, 024417 (2004).
[42] Z. Li and S. Zhang, Phys. Rev. Lett. **92**, 207203 (2004).
[43] A. Thiaville, Y. Nakatani, J. Miltat, and Y. Suzuki, Europhys. Lett. **69**, 990 (2005).
[44] A. Thiaville, Y. Nakatani, F. Piéchon, J. Miltat, and T. Ono, Eur. Phys. J. B **60**, 15 (2007).
[45] E. Martinez, L. Lopez-Diaz, O. Alejos, L. Torres, and M. Carpentieri, Phys. Rev. B **79**, 094430 (2009).
[46] C. T. Boone and I. N. Krivorotov, Phys. Rev. Lett. **104**, 167205 (2010).
[47] P. Chureemart, R. F. L. Evans, and R. W. Chantrell, Phys. Rev. B **83**, 184416 (2011).
[48] J. Iwasaki, M. Mochizuki, and N. Nagaosa, Nat. Nanotechnol. **8**, 742 (2013).
[49] J. Sampaio, V. Cros, S. Rohart, A. Thiaville, and A. Fert, Nat. Nanotechnol. **8**, 839 (2013).
[50] M. D. Petrović, B. S. Popescu, U. Bajpai, P. Plecháč, and B. K. Nikolić, Phys. Rev. Appl. **10**, 054038 (2018).
[51] G. Stefanucci and R. van Leeuwen, *Nonequilibrium Many-Body Theory of Quantum Systems: A Modern Introduction* (Cambridge University Press, Cambridge, 2013).
[52] B. Gaury, J. Weston, M. Santin, M. Houzet, C. Groth, and X. Waintal, Phys. Rep. **534**, 1 (2014).
[53] S. E. Barnes and S. Maekawa, Phys. Rev. Lett. **98**, 246601 (2007).
[54] J.-I. Ohe and S. Maekawa, J. Appl. Phys. **105**, 07C706 (2009).
[55] Y. Shimada and J.-I. Ohe, Phys. Rev. B **91**, 174437 (2015).
[56] Y. Yamane, J. Ieda, and J. Sinova, Phys. Rev. B **93**, 180408 (2016).
[57] A. Croy and U. Saalmann, Phys. Rev. B **80**, 245311 (2009).
[58] B. S. Popescu and A. Croy, New J. Phys. **18**, 093044 (2016).
[59] H.-P. Breuer and F. Petruccione, *The Theory of Open Quantum Systems* (Oxford University Press, Oxford, 2002).
[60] S. Zhang and Z. Li, Phys. Rev. Lett. **93**, 127204 (2004).
[61] Y. Zhao, Y. Liu, H. Tang, H. Jiang, Z. Yuan, and K. Xia, Phys. Rev. B **98**, 174412 (2018).
[62] A. Brataas, Y. Tserkovnyak, and G. E. W. Bauer, Phys. Rev. B **84**, 054416 (2011).
[63] J. Fransson, Phys. Rev. B **82**, 180411 (2010).
[64] T. Saygun, J. Bylin, H. Hammar, and J. Fransson, Nano Lett. **16**, 2824 (2016).
[65] T. Taniguchi, K.-J. Kim, T. Tono, T. Moriyama, Y. Nakatani, and T. Ono, Appl. Phys. Express **8**, 073008 (2015).
[66] L. Berger, Phys. Rev. B **33**, 1572 (1986).
[67] G. E. Volovik, J. Phys. C **20**, L83 (1987).
[68] A. Stern, Phys. Rev. Lett. **68**, 1022 (1992).
[69] R. A. Duine, Phys. Rev. B **77**, 014409 (2008).
[70] Y. Tserkovnyak and M. Mecklenburg, Phys. Rev. B **77**, 134407 (2008).
[71] S. A. Yang, G. S. D. Beach, C. Knutson, D. Xiao, Q. Niu, M. Tsoi, and J. L. Erskine, Phys. Rev. Lett. **102**, 067201 (2009).
[72] F. Freimuth, S Blügel, and Y. Mokrousov, arXiv:1806.04782.
[73] M. Sayad, R. Rausch, and M. Potthoff, Phys. Rev. Lett. **117**, 127201 (2016).
[74] P. Mondal, U. Bajpai, M. D. Petrović, P. Plecháč, and B. K. Nikolić, Phys. Rev. B **99**, 094431 (2019).
[75] F. Mahfouzi and B. K. Nikolić, Phys. Rev. B **90**, 045115 (2014).
[76] H.-T. Elze, Phys. Rev. A **85**, 052109 (2012).
[77] J. Weston and X. Waintal, Phys. Rev. B **93**, 134506 (2016).